Making continental crust on water-bearing terrestrial planets

Justine Bernadet, Anastassia Yu. Borisova, Martin Guitreau, Oleg Safonov, Paul Asimow, Anne Nédélec, Wendy Bohrson, Svetlana Kosova, Philippe de Parseval

SPACE SCIENCES

Making continental crust on water-bearing terrestrial planets

Justine Bernadet[1], Anastassia Y. Borisova[1]*, Martin Guitreau[2], Oleg G. Safonov[3,4], Paul Asimow[5], Anne Nédélec[1], Wendy A. Bohrson[6], Svetlana A. Kosova[4], Philippe de Parseval[1]

The debate about early Earth differentiation focuses on the processes responsible for the formation of protocrust(s) and continental crust of felsic ($SiO_2 \geq 55$ weight %) composition. One aspect of this debate is how Hadean zircons fit into an ultramafic environment. On the basis of experiments, thermodynamic modeling, and elemental partitioning, we show that felsic melts could have been generated by shallow interaction between primordial serpentinized peridotite and basaltic magmas on Earth and Mars. On the basis of the hafnium isotopic evolution of Hadean detrital zircons worldwide, we infer that these interactions allowed for the formation of extensive Hadean felsic crust (4.4 to 4.5 billion years ago), which, in turn, would account for up to 50% of the present continental crustal mass. A similar process may have occurred on Mars. The serpentinized protocrust had a dual role in the primitive planetary environment: to provide ingredients for the continental crust and to enable life to emerge on water-bearing terrestrial planets.

INTRODUCTION

It has long been recognized that the Earth's continental crust is Si and Al rich [i.e., ~60 wt % SiO_2 and ~15 wt % Al_2O_3; (*1*)] and is thus felsic, as testified to by the archaic adjective "sialic." The presence of continental crust on Earth is considered to be a consequence of plate tectonics and abundant liquid water (*2*). Current geodynamic models predict that liquid-water oceans could be generated on planetary surfaces under a wide range of conditions (*3*), such that the continental crust could also be present on other rocky planets such as Mars (*4*). The only remaining witnesses of the Hadean Eon are fossil isotopic signatures left by extinct radioactivity (e.g., μ^{142}Nd and μ^{182}W) and detrital zircon crystals ($ZrSiO_4$) found in a dozen locations (*5*). Extinct radioactivity mostly indicates that primordial protocrusts were mafic and that mantle depletion was widespread and started early, >4.3 billion years ago (Ga) (*5*). In contrast, Hadean zircon crystals point to the existence of felsic magmas, crustal reworking, relatively cool and oxidizing crustal conditions, and surface weathering linked to liquid water and suggest that life may have had already emerged by 4.1 Ga (*6*–*11*). These primordial conditions possibly occurred on other terrestrial planets and exoplanets as well. Ancient quartz diorite or granodioritic rocks have been identified in situ on Mars (*12*, *13*), and evidence for early felsic rocks has been reported by remote observations thanks to spectroscopy (*4*, *14*–*17*) by Compact Reconnaissance Imaging Spectrometer for Mars (CRISM) and Galileo Near-Infrared Mapping Spectrometer data for Venus. Continental crust formation is generally assumed to be intimately linked to plate tectonics on Earth (*5*), but it is hard to reconcile the presence of continental crust on other planets that exhibit no evidence for such a geodynamic regime.

Geochemical constraints such as detrital zircon Hf isotope compositions imply that Hadean felsic crust production began as early as 4.5 billion years (Gyr) ago (*18*, *19*). Recently, we proposed a previously unknown mechanism for plagiogranite crust production via shallow, fluid-assisted interaction between heavily serpentinized protocrust and basaltic melts (*20*, *21*). In the present manuscript, we document the maximum mass of felsic crust produced by serpentinite-basaltic melt interaction and estimate the thermodynamic stability of a primordial continental crust produced by this mechanism. In addition, we present an original model of primordial primitive mantle magma ocean-to-felsic protocrust differentiation based on the thermodynamic modeling for Earth and Mars. All experimental, analytical, and modeling data are given in figs. S1 to S7 and tables S1 to S25.

RESULTS

To constrain trace element compositions of the resulting melt (e.g., Lu/Hf, Rb/Sr, Sm/Nd, and U) and olivine, we performed 13 long-duration experiments on Earth's basalt-serpentinite interaction (fig. S1) and conducted temperature-pressure (*T*-*P*)–controlled thermodynamic modeling to constrain the physical-chemical conditions and mass of shallow felsic crust production on Earth and Mars. The experiments (with variable melt-to-rock mass ratio, *R*) were designed to simulate open-system interaction of basaltic melts with surrounding serpentinite. The coupled basalt-serpentinite system does not necessarily have to reach thermodynamic equilibrium, although this is likely to be the case in the experiments carried out previously (*20*) and in this work (table S1). All experimental, analytical, and modeling details are shown in Materials and Methods. The produced mafic to felsic melt compositions and the melt fractions strongly depend on the starting basaltic melt-to-serpentinite mass ratio (Fig. 1). The ~6 wt % difference between SiO_2 contents obtained in the models and those measured in experimental melts are explained by a contribution from shallow supercritical aqueous fluid produced in the hybrid system (*20*). The resulting mafic to felsic melts [Mg# = Mg/(Mg+Fe) ≥ 40] coexist with a garnet-free residue composed mostly of high-Mg

[1]Géosciences Environnement Toulouse, GET, Université de Toulouse, CNRS, IRD, UPS, France, 14 Avenue E. Belin, 31400 Toulouse, France. [2]Laboratoire Magmas et Volcans, CNRS-UMR6524, IRD-UMR163, OPGC, Université Clermont Auvergne, F- 63178 Aubière, France. [3]Department of Geology, University of Johannesburg, Johannesburg, South Africa. [4]Korzhinskii Institute of Experimental Mineralogy, 142432 Chernogolovka, Moscow Region, Russia. [5]California Institute of Technology, 1200 East California Boulevard, Pasadena, CA 91125, USA. [6]Department of Geology and Geological Engineering, Colorado School of Mines, Golden, CO 80401, USA.
*Corresponding author. Email: anastassia.borisova@get.omp.eu, anastassiafr@yahoo.fr

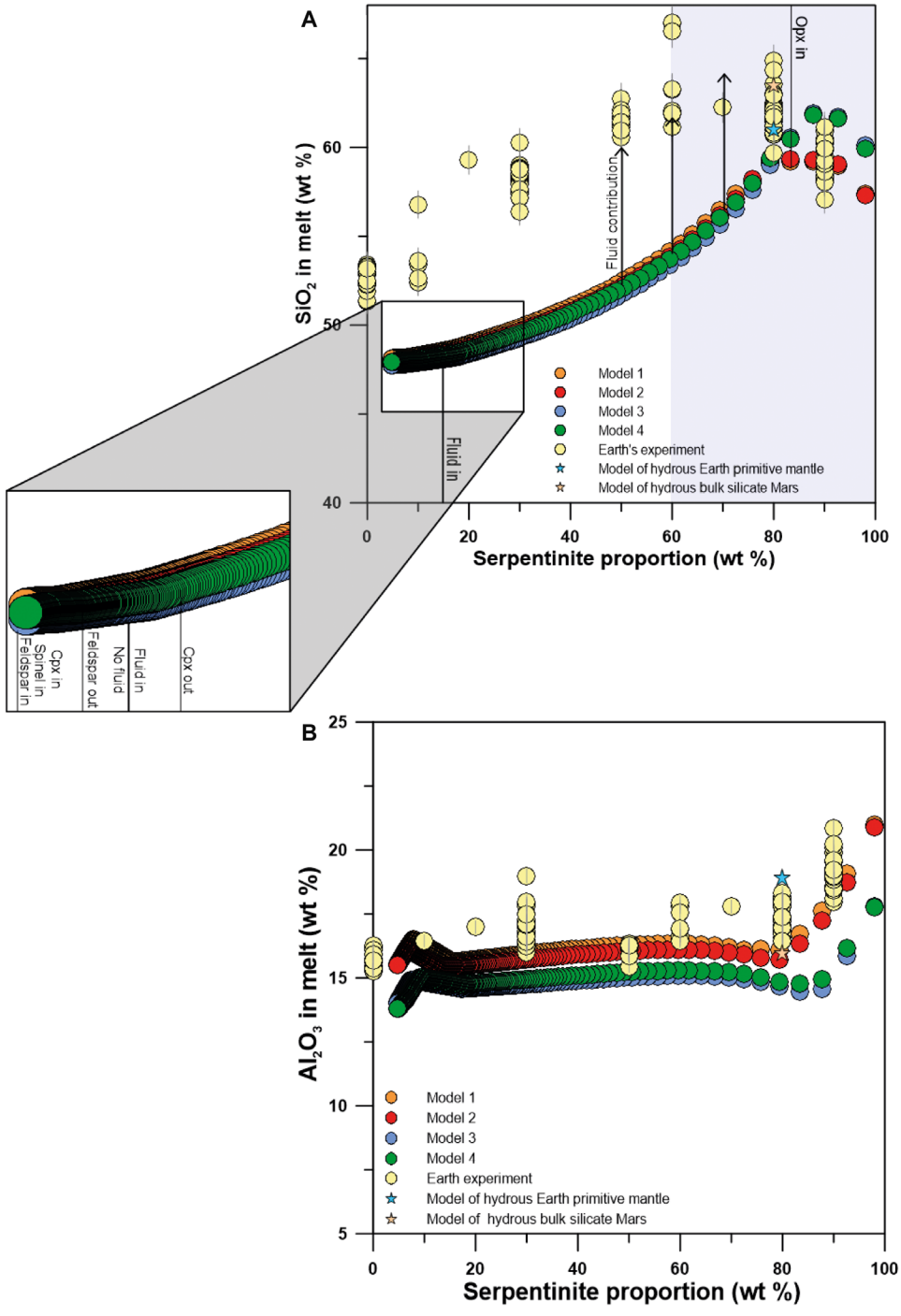

Fig. 1. Felsic glasses and melts produced during experiments and by MELTS modeling. (**A** and **B**) SiO_2 and Al_2O_3 contents (in wt %) in the resulting melts versus starting serpentinite proportions (or percentage in wt %) produced in the basalt-serpentinite system based on rhyolite-MELTS thermodynamic modeling and the 0.1-GPa experiments. On the basis of the thermodynamic modeling, we show that felsic ($SiO_2 \geq 55$ wt %) melts could have been generated by shallow basalt-serpentinite interaction on Earth. The shaded area corresponds to the most relevant serpentinite proportions (≥60 wt %) when the melt compositions are felsic. The 6 wt % SiO_2 difference between SiO_2 contents in the modeled and experimental (yellow symbols) melts is explained by the role of supercritical aqueous fluid (*19*). Model 1 at 1090°C and 0.1 GPa and model 2 at 1100°C and 0.1 GPa are performed with 1.0.2 MELTS. Model 3 at 1110°C and 0.1 GPa and model 4 at 1090°C and 0.1 GPa are obtained with 1.0.2 MELTS and 1.2.0 MELTS, respectively. The experiment was performed at 1100°C and 0.1 GPa. The stars correspond to the partial melts reaching felsic composition produced when the Earth's primitive mantle or the Bulk Silicate Mars are reequilibrated at 950° to 1000°C and 0.1 GPa. Cpx, clinopyroxene. All data are available in tables S7 to S25.

olivine (Fo ≥ 91 mol %, forsterite content), rare Cr-spinel [Mg# = Mg/(Mg+Fe) ≥ 50, Cr# = Cr/(Cr+Al) ≥ 60], and rare high-Mg clino- and orthopyroxenes [Mg# = Mg/(Mg+Fe) ≥ 68] (table S2). Heating of pure serpentinite (100 wt %) to basalt superliquidus temperatures does not generate melt but does produce an aqueous fluid in equilibrium with a harzburgite residue (figs. S2 to S4). The optimal serpentinite percentage favorable for felsic melt production (SiO_2 > 55 wt %) varies between 60 and 99 wt % (Fig. 1). The fraction of felsic melt that is plagiogranite-type at the most relevant serpentinite percentage is inversely proportional to the starting serpentinite percentage (in wt %) in the basalt-serpentinite system (e.g., high serpentinite proportions yield low portions of melt; Fig. 2). An important outcome of our experiments is also the fact that the more serpentinite involved, and hence the more hydrated the protocrust, the more enriched in trace elements is the produced felsic melts, except for U (fig. S6). U was the most efficient heat-producing element, through ^{235}U decay, during the Hadean Eon. Consequently, the shallow upper mantle could maintain high heat flux, which, in turn, would influence the rheology of the upper mantle, preventing it from stiffening and initiating plate tectonics-like regime.

Our rhyolite-MELTS (versions 1.0.2 and 1.2.0) thermodynamic calculations of felsic (Fig. 1, ≥55 wt % SiO_2; figs. S2 to S4; and tables S7 to S25) melt stability and melt fractions (Fig. 2) produced through the basalt-to-serpentinite reaction were done at 1090° to 1250°C and 0.1 to 0.7 GPa, as well as redox conditions corresponding to quartz-fayalite-magnetite (QFM) mineral buffer. These calculations constrain the maximum mass of the primordial continental crust compared to that of the bulk continental crust on Earth (*22*), and felsic melt fractions were further used to constrain the bulk mass of the felsic crust. These masses are minima because we only used rhyolite-MELTS model data, which showed an ~6 wt % difference between SiO_2 contents obtained in models and those measured in experimental melts; these differences can be explained by contribution from a shallow supercritical aqueous fluid (*20*). These constraints indicate that felsic crust production is possible owing to the shallow (≤0.5 GPa, <20 km) reaction between primordial hydrated peridotite and basalt at the beginning of the Hadean (4.4 to 4.5 Ga). We demonstrate that it was possible to produce felsic (continental) crust equivalent to a minimum of 50% of present-day continental crust mass (table S6).

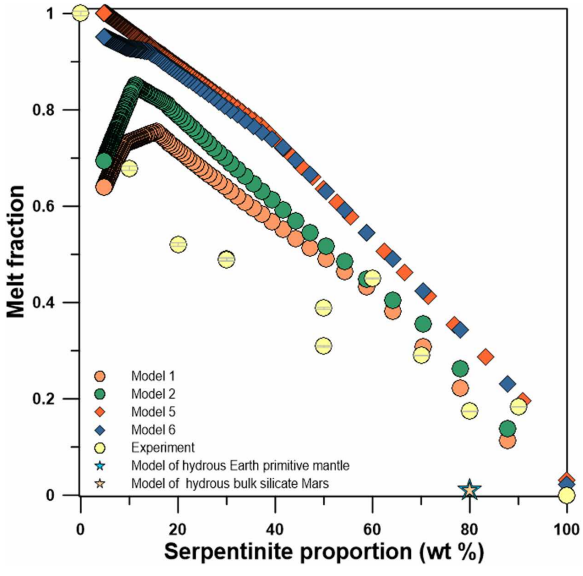

Fig. 2. Resulting melt fraction versus starting serpentinite proportion (or percentage in wt %) in the basalt-serpentinite system from 0.1 to 0.7 GPa and from 1090° to 1250°C. The rhyolite-MELTS thermodynamic calculations of melt fractions (<0.4) of felsic (≥ 55 wt % SiO_2) melts produced due to the Earth's basalt-to-serpentinite reaction at 1090° to 1250°C and 0.1–0.7 GPa constrain the maximal mass of the primordial continental crust. Model 5 at 1250°C and 0.5 GPa and model 6 at 1250°C and 0.7 GPa are obtained with 1.2.0 MELTS and 1.0.2 MELTS, respectively. For experimental and other modeling constraints, see caption to Fig. 1. All data are available in tables S1 and S7 to S25.

DISCUSSION

Trace element [e.g., rare earth elements (REEs), Hf, etc.] concentrations in experimentally produced felsic glasses from this study allow constraints to be placed upon early mantle-crust differentiation processes, which were encoded in Hadean zircons. Because the resulting felsic glass composition is controlled by that of the starting basaltic melt, the resulting glass is moderately enriched in REEs, Hf, Zr, and other lithophile elements. Figure 3 presents a relevant compilation of $\varepsilon_{Hf(T)}$ versus age [million years ago (Ma)] for Hadean and Archean zircons (*18*, *19*, *23*–*28*). Hafnium isotope signatures in Hadean zircons define a broad positive correlation with age as already noted by several authors [e.g., (*8*, *19*, *23*, *25*)]. This broad correlation is commonly interpreted as tracing the reworking of an isolated enriched reservoir throughout the Hadean. The slope of this correlation can be converted into a Lu/Hf ratio which, in turn, can be used to establish the nature of the enriched reservoir that was the source of zircon parental magmas. When converted into a Lu/Hf ratio, the correlation for Hadean zircons gives an average $^{176}Lu/^{177}Hf$ of ~0.02 [e.g., (*19*, *25*)]. This ratio, taken at face value, is interpreted as tracing a "mafic" crust involvement and reworking (*18*, *19*, *23*, *25*) because mafic rocks generally exhibit these values (*29*). Our experimental felsic glasses produced at 0.1 to 0.2 GPa (≤6 km in depth; tables S3 and S4) have a variable Lu/Hf of 0.08 to 0.17 (fig. S5), equivalent to a $^{176}Lu/^{177}Hf$ of 0.011 to 0.024, which are identical to that recorded by Hadean zircons. In our experiments, the highest ratios ($^{176}Lu/^{177}Hf$ = 0.023 to 0.024), which were obtained in 8 of 11 experiments (72%), correspond to felsic rather than mafic melts. This finding addresses a major controversy, which is that mafic crust reworking cannot explain the affinity of many Hadean zircons that belong to meta- to peraluminous granites (high-Al composition with aluminum saturation index ≥ 1) (*5*, *10*, *27*). Therefore, meta- to peraluminous felsic melts derived from hydrated ultramafic protocrust and their further reworking throughout the Hadean can account for all features of Hadean zircons. This felsic crust differentiation process could have started 4.5 Gyr ago and required prior alteration of the early-solidified magma ocean by liquid water.

It has been proposed that the correlation exhibited by Hadean zircons may reflect a more complex history of mafic and felsic crust reworking (*30*) and that it may also be affected by analytical and/or geological artifacts (*31*). Consequently, more than one process could be hidden in the broad Hadean correlation of Fig. 3 but it is essentially impossible to deconvolute this complexity at the scale of analytical uncertainties. However, such $\varepsilon_{Hf(T)}$ versus age correlation at a crustal scale is known to be apparently controlled, and buffered, by dominant lithologies [e.g., (*32*, *33*)]. Consequently, the average $^{176}Lu/^{177}Hf$ obtained from such correlations may not fully capture the complexity of crustal evolution but may still provide meaningful

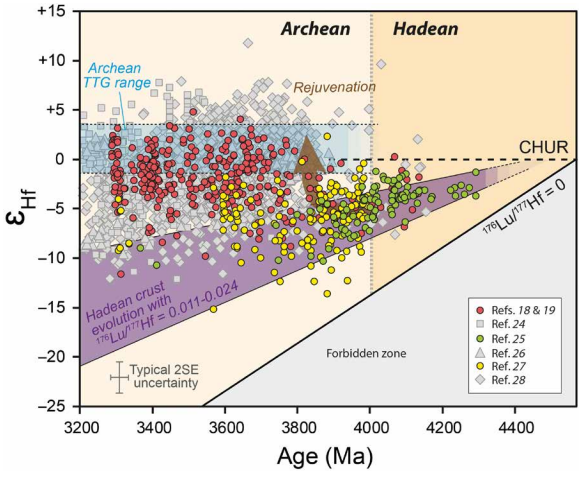

Fig. 3. εHf versus age for globally distributed early terrestrial zircons. This plot shows the specific evolution of Hadean zircon crystals, illustrated by the purple array, compared to Archean crystals, which have more variable signatures requiring an interplay between mantle contribution (rejuvenation) and crustal reworking. All symbols correspond to zircon data. The data represent the evolution of reservoirs characterized by $^{176}Lu/^{177}Hf$ that commonly correspond to chondritic 0.0338 (*60*), basaltic 0.022 (*23*), felsic 0.012 (*7*), and TTG (tonalite-trondhjemite-granodiorite) 0.004 (*61*). The Archean TTG range is after (*61*). Our results illustrate that Hadean zircon parental magmas may have originated from reworking of felsic Hadean crust characterized by $^{176}Lu/^{177}Hf$ obtained in our experiments (0.011 to 0.024), which was not the case in post-Hadean processes, where this crust appears no longer sampled. The brown arrow represents post-Hadean rejuvenation by crust-to-mantle interaction.

insights into dominant crustal processes. The results of our experiments, therefore, provide a viable interpretation of Hadean zircon $\varepsilon_{Hf(T)}$ versus age correlation. We further show that the reworking of such a felsic reservoir could be detected in the early Sr isotope record but not in the Nd isotope record due to very limited fractionation between Sm and Nd (fig. S7).

Widespread melting of hydrated peridotite protocrust is possible not only due to initial (ultra)mafic magmatism but also due to meteoritic impact-induced melting (*20*, *34*). Our model limits the maximum pressure of felsic crust formation at 0.5 GPa, which corresponds to a depth of 18 km on Earth (Fig. 4). Zircon-bearing plagiogranites (*20*, *21*) were formed due to high-temperature reactions, and 18 km is the thermodynamic limit for such primordial plagiogranite crust production provided that protocrust was hydrated and fractured to these depths and conditions close to equilibrium conditions were achieved during high-temperature fluid-assisted reactions (Figs. 1 and 2, figs. S2 to S4, and table S6). Extensive melting of protocrust could, hence, be possible at the beginning of the Hadean, where residual basaltic melts from a magma ocean percolated through solidified ultramafic protocrust. Renewed melting of the ultramafic protocrust or reworking of the early felsic crust could still occur due to low to moderate velocity impacts during the early Hadean. The zircon-bearing plagiogranites (*20*) or granitic (*35*) crust was likely produced in high volume during the Hadean. Available models on impact-induced melting at controlled velocity of the impacting bodies (*36*) predict that shallow impact-induced melting related to low to moderate velocity (≤20 km/s) and high-density impacts could be a principal trigger of widespread partial melting. This process can be responsible for the formation of a crustal volume that corresponds to a maximum of ~50% of present-day felsic crust, which would have segregated from the ultramafic residue at the beginning of planetary evolution according to this study (Fig. 4 and table S6). As we consider the planetary surface to be covered by primordial hydrated (ultra)mafic protocrust, impact-induced melting is a likely process for formation of primordial shallow plagiogranite crust during the Hadean.

Alternatively, primordial differentiation of an ultramafic primitive mantle–type magma ocean during the early Hadean could account for shallow plagiogranite protocrust production provided that extensive volatile element degassing occurred and aqueous fluid saturation conditions occurred at shallow levels upon magma ocean differentiation and cooling (Figs. 1 and 2). Thermodynamic equilibration at 1000°C and 0.1 GPa of the Earth's primitive mantle would result in felsic melt production (Fig. 4). Water saturation of the magma ocean at shallow levels is highly possible based on physical considerations (*37*). The bulk hybrid system of basalt with hydrated harzburgite (serpentinite) is similar to the initial primitive mantle–type model composition (~80 wt % harzburgite +20 wt % basalt) (*38*). Our model of shallow (<10 km) differentiation under water-saturated and moderate-temperature (1000°C) conditions (Fig. 1) followed by melt segregation from an ultramafic residue at the beginning of the Hadean could have produced <1% of present-day continental crust mass (Fig. 4 and table S6). However, this is a minimum estimate because we only considered shallow levels of the primitive mantle layers and static instead of dynamic (convection-driven) differentiation. Therefore, the limited production of continental protocrust could have been possible at the very beginning of planetary evolution (early Hadean, 4.4 to 4.5 Ga) and could generate continental crust (<1 km in depth) from shallow hydrated primitive mantle magma ocean material provided high water contents at shallow levels that allowed aqueous fluid saturation of the magma at pressures below 0.1 GPa. This process of felsic protocrust differentiation, which may have happened as early as 4.5 Ga, requires earlier hydration of the shallow magma ocean by an aqueous fluid.

The above-described mechanisms may have also been effective on Mars during the Pre-Noachian to Noachian. Martian serpentinites have been detected in ancient terrains (*39*), likely indicating hydrothermal activity and serpentinite production even if an ocean eventually formed on Mars (*40*), and that the Martian mid-crust was composed of rocks saturated with an aqueous fluid (*41*). The presence of serpentinite implies an essential role of hydrothermal activity in the past on Mars. The bulk silicate composition of the Martian mantle differs from that of the Earth's mantle due to a much higher FeO content, up to 15 wt % (*42*), which explains the higher density of the Martian mantle. Model input of primitive basalt and serpentinite compositions are representative for Mars, and the thermodynamic modeling procedure is the same as that applied for the Earth's felsic crust (Materials and Methods and table S1). Impact-induced melting of serpentinized protocrust impregnated with basalt below 0.4 GPa may be responsible for up to ~40% of Martian felsic crust formation and segregation from the ultramafic residue at the beginning of planetary evolution (Fig. 4 and table S6), assuming a 30-km-thick modern Martian crust (*43*).

Alternatively, planetary differentiation and the first felsic protocrust production could happen during the solidification of a magma ocean that has primitive mantle composition. To account for the existence of evolved felsic lithologies (granodiorites) and thick crustal blocks observed at the Martian surface through rover and orbiter

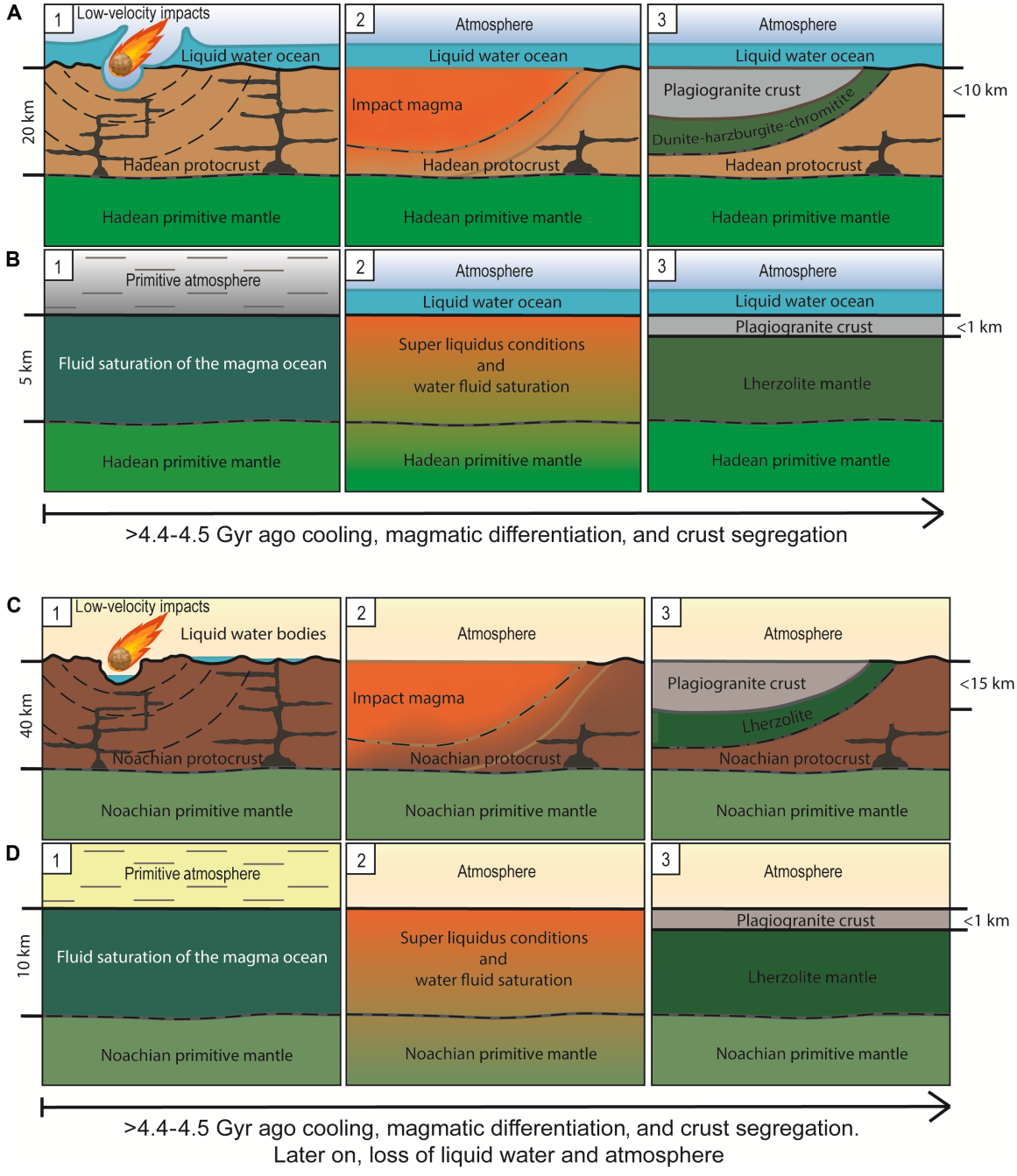

Fig. 4. Schematic illustration of scenarios of the felsic crust and protocrust formation. (**A**) Scenario relates the abundant Earth's felsic crust formation to extensive impact-induced melting of serpentinized protocrust during Hadean, whereas scenario (**B**) relates the limited Earth's felsic protocrust production to primitive magma ocean differentiation. Schematic illustration of (**C**) and (**D**), two scenarios of the Martian felsic crust and felsic protocrust formation, respectively. (C) Scenario relates the abundant Martian felsic crust formation to extensive impact-induced melting of the serpentinized protocrust, whereas scenario (D) relates the limited felsic Martian protocrust production to primordial magma ocean differentiation. All starting material component compositions can be found in the table S1B. The models are explained in Materials and Methods and summarized in tables S6 to S25.

analysis (*4*, *12*, *13*), we performed thermodynamic modeling of bulk silicate Mars at moderate depths with aqueous fluid saturation. Shallow-level differentiation (at 0.1 GPa corresponding to ≤10 km in depth; table S6) could happen at conditions of aqueous fluid saturation and a temperature of 950°C (Figs. 1 and 4). The subsequent segregation of the felsic melt from an ultramafic residue at depths below 1 km at the beginning of the Pre-Noachian could account for <1% of the bulk Martian continental crust (table S6). Again, this is a minimum estimate because we only considered shallow levels of the water-saturated primitive mantle and a static instead of dynamic differentiation. Figures 1 and 4 illustrate that low-pressure silicate and hydrous mantle differentiation could be a viable rock-forming

process to produce a limited felsic protocrust on terrestrial planets such as Mars.

Extensive formation of felsic crust could happen due to the presence on rocky planets of highly serpentinized protocrust, whereas only limited felsic protocrust could be produced from primitive magma ocean differentiation. In addition to providing the means of formation of the first felsic crust, shallow serpentinite protocrust is also a favorable setting for the abiotic synthesis of amino acids/RNA components in shallow hydrothermal systems (*44*), creating an appropriate tectono-magmatic environment for the emergence of life on Earth and possibly on other water-bearing terrestrial planets.

MATERIALS AND METHODS

High-temperature experiments

Mixed-type long-duration reaction experiments were used to model equilibration. The starting materials were composed of mixtures of basalt and serpentinite powders in different proportions (from 0 to 100 wt % of serpentinite; Fig. 1), and therefore different starting melt (basaltic component)-to-rock (serpentinite component) mass ratios (*R*, in wt %) were used (table S1A). The starting serpentinite and basalt compositions are given in the table S1B. The starting basalt is a slightly enriched mid-ocean ridge basaltic glass with composition corresponding to the Archaean basalt (*21*). Experiments were performed at 0.1 GPa and 1100°C, and all experiments were run for 5 days. The experiments (with variable melt-to-rock mass ratio, *R*) were designed to simulate open-system interaction of basaltic melt with serpentinite. The hybrid system does not necessarily have to reach thermodynamic equilibrium, although this is likely to be the case in the experiments carried out in this work. The 6 wt % difference between SiO_2 contents in the modeled and experimental melts (Fig. 1) is explained by the contribution of aqueous fluid (*20*), which cannot be distinguished from melt due to the quenching effect. The experiments were carried out using an internally heated gas pressure vessel at the Korzhinskii Institute of Experimental Mineralogy, Chernogolovka, Russia, using argon gas as the pressure medium. The system was heated by a furnace with two windings (to minimize the thermal gradients). The temperature was controlled and measured by a TRM-101 OVEN controller with two S-type ($Pt_{90}Rh_{10}$-Pt_{100}) thermocouples. The thermocouples were mounted on top and close to the bottom of the experimental capsule. The experiments were quenched by switching off the furnace's electrical power. The pressure during the quench was constant down to 150°C and then was slowly released at lower temperatures. The cooling rate from the run temperature to 500°C was 167°C/min and 90°C/min down to 150°C.

Microanalysis

Major element analyses of silicate and oxide minerals and silicate glasses (table S2) and backscattered electron images of the samples were performed at the Géosciences Environnement Toulouse (GET, Toulouse, France) laboratory and at the Centre de Microcaractérisation Raimond Castaing (Toulouse, France). The main silicate phases in the samples were identified using a scanning electron microscope JEOL JSM-6360 LV coupled with energy-dispersive x-ray spectroscopy (*20*). The major, minor, and volatile element concentrations in glasses and minerals were analyzed using a CAMECA SX-Five microprobe. For the microanalysis of the silicate hydrous glasses, the CAMECA SX-Five was used following the method in (*20*). The beam (15 kV and 10 nA) was defocused to ~10 μm^2 where possible for the glass analysis. Sodium was analyzed first to ensure minimal loss during electron probe microanalysis (EPMA). For the microanalysis of the silicate and oxide minerals, the beam (15 kV and 20 nA) was focused to ~2 μm^2. These analytical conditions allowed an optimal signal for the major and minor elements, good internal precision, and minimal sodium loss during EPMA. The following synthetic and natural standards were used for calibration: albite (Na), corundum (Al), wollastonite (Si and Ca), sanidine (K), pyrophanite (Mn and Ti), hematite (Fe), periclase (Mg), and Cr_2O_3 (Cr). Element and background counting times for most analyzed elements were 10 s (except for 5 s for Na and K) and 5 s, respectively, whereas the peak counting time was 120 s for Cr. The detection limit for Cr was 70 parts per million. The silicate reference materials of MPI-DING and SRM NIST, which ranged from ultramafic to felsic composition (GOR132-G, GOR128-G, KL2-G, ML3B-G, and ATHO-G) (*45*), were analyzed as unknown samples to monitor analytical accuracy. The estimated accuracy ranges from 0.5 to 3% [1σ RSD (relative SD)], depending on the element contents in the reference glasses. In addition, analysis of reference silicate material allowed us to estimate analytical precision for the major and minor elements (e.g., Cr in glasses). The precision estimated in this way is compatible with the microprobe analytical uncertainty (derived from counting statistics).

Experimental glass compositions were determined using laser ablation inductively coupled plasma mass spectrometry at Laboratoire Magmas et Volcans (Clermont-Ferrand, France) using a Resonetics Resolution M-50 (5-ns pulse duration and 193-nm wavelength) coupled to a Thermo Element XR. Measurements were conducted using a spot size of 15 μm, a frequency of 3 Hz, and a fluence of 2.5 J/cm^2. We analyzed the following interference-free isotopes to determine elemental concentrations: ^{11}B, ^{23}Na, ^{25}Mg, ^{27}Al, ^{29}Si, ^{39}K, ^{43}Ca, ^{49}Ti, ^{55}Mn, ^{85}Rb, ^{88}Sr, ^{89}Y, ^{90}Zr, ^{93}Nb, ^{133}Cs, ^{138}Ba, ^{139}La, ^{140}Ce, ^{141}Pr, ^{146}Nd, ^{147}Sm, ^{151}Eu, ^{157}Gd, ^{159}Tb, ^{163}Dy, ^{165}Ho, ^{166}Er, ^{169}Tm, ^{173}Yb, ^{175}Lu, ^{180}Hf, ^{181}Ta, ^{183}W, ^{208}Pb, ^{232}Th, and ^{238}U. Experimental glasses were analyzed by standard bracketing using SRM NIST 612 (*45*), which was used as our primary reference material, whereas BCR-2G (*46*) was used as a secondary standard for quality check. Concentrations were obtained from background-corrected signals using ^{43}Ca, and data were processed using the software GLITTER (*47*, *48*). All determined concentrations are consistent with published uncertainty, which is <20%.

Thermodynamic modeling

Calculations used an enriched mid-ocean ridge basalt sample as a representative mafic melt and the serpentinite TSL-19 (*19*) as the representative serpentinite rock for Earth and typical Martian or comparable terrestrial analogs for basalt and serpentinite for Mars (table S1B). The starting materials of Martian serpentinite and basalt, Bulk Silicate Mars, and Earth's primitive Mantle are from refs. (*38*, *42*, *43*, *49*–*51*) (table S1B). To estimate the composition of the melt and mineral phases produced in serpentinite-basalt interaction, we performed rhyolite-MELTS thermodynamic equilibrium calculations in the basalt-serpentinite system. Most calculations were conducted at a temperature range from 1100° to 1250°C and pressures of 0.1 to 0.7 GPa and oxygen fugacity corresponding to QFM oxygen mineral buffer, with basalt-to-serpentinite initial mass ratios (*R*) covering the whole range of the experimental ratios in the mixed experiments where the felsic liquids were recorded. Initial basaltic melt-to-serpentinite rock mass ratios (*R*) ranged from 0 to

1. Modeling of thermodynamic equilibrium phases was performed using the easyMelts 0.2.4 beta (https://magmasource.caltech.edu/gitlist/easyMelts.git/) software package and rhyolite-MELTS (versions 1.2.0 and 1.0.2) software (*52*, *53*). During the modeling of interaction between a pure serpentinite end-member and a basaltic melt, the rate of assimilation was 2 g per step for 1000 steps; tables S7 to S25 list modeling results, and figs. S2 to S4 provide more information on the performed PERPLE_X thermodynamic modeling.

PERPLE_X modeling (version 7.1.5, published 12 January 2023) was also used to further compare thermodynamic model results to the experimental data. The database was set to hp633ver.dat, and computational option was left to default. The main oxide components were left untransformed. The goal for this study was to create a two-dimensional grid, with a starting serpentinite mass fraction from 0 to 1 (from 0 to 100 wt %) on the *x* axis whereas temperatures ranging from 1173 K (900°C) to 1673 K (1400°C) on the *y* axis of phase diagrams. Fluid equation of state used was that in (*54*), and solid solution list used accounts for the presence of clinopyroxene, orthopyroxene, spinel, olivine phases all from (*55*), as well as plagioclase, ilmenite (*54*), and melt (*56*) in the hybrid system. An optimal terrestrial serpentinite percentage favorable for production of felsic (≥55 wt % SiO_2) melts is higher than 60 wt % at a melt fraction lower than 0.4. Thus, it was confirmed that optimal parameters for the felsic (≥55 wt %) melt production were between 0.1 and 0.2 GPa, temperatures between 1273 and 1473 K (1000° and 1200°C), and starting hydrated peridotite proportions above 60 wt %. Further phase diagrams were thus created first by using a fixed mixture of 80 wt % serpentinite and 20 wt % basalt ratio, plotting pressure against temperature. Two additional diagrams were then created plotting compositions against pressure on a fixed temperature of 1373 K (1100°C), and one representing composition versus temperature using the fixed pressures of 0.2 GPa (figs. S2 to S4).

Geochemical modeling

Theoretical modeling of the Lu-Hf evolution corresponds to the isotopic notations of $\varepsilon_{Hf}(T)$

$$\varepsilon_{Hf(T)} = \left\{ \left[\left({}^{176}Hf/{}^{177}Hf \right)_{sample} / \left({}^{176}Hf/{}^{177}Hf \right)_{CHUR} \right] - 1 \right\} \times 10^4 \quad (1)$$

where CHUR is chondritic uniform reservoir. The CHUR (Chondritic Uniform Reservoir) $^{176}Hf/^{177}Hf$ ratio was corrected using a present-day value of 0.282793 and a $^{176}Lu/^{177}Hf$ ratio of 0.0338 (*57*). The felsic crust differentiation line corresponds to the average Lu/Hf = 0.16 and $^{176}Lu/^{177}Hf = 0.023$ observed in the basalt-serpentinite reaction-type experiments (Fig. 3). To plot the line, the decay constant $\lambda\ ^{176}Lu = 1.867.10^{11}$ year^{-1} (*58*) and chondritic uniform reservoir parameters published in (*57*) were used.

Estimation of the continental crust and protocrust masses and depths (Earth and Mars)

The protocrust is formed due to the magma ocean solidification. Masses (kg and tonne) of the continental crusts and protocrusts (Earth, Mars) were estimated using the following equation

$$M = 4\pi\, F\, R^2\, H\, \rho \quad (2)$$

where *M* is the continental crust mass (kg and tonne), *F* is the maximum fraction of felsic melt obtained by the performed thermodynamic modeling, *R* is the Earth's radius (and Martian radius) (*59*) (km), *H* (km) is the maximum depth where the shallow felsic (>55 wt % SiO_2) crust is stable, and ρ (kg/m^3) is the average density of the felsic crusts (*49*) (table S6). The obtained continental crust masses were subsequently compared to the mass of the modern Earth's continental crust (*22*) and the bulk mass of the Martian continental crust (~1.3^{19} tonnes) estimated based on the available InSight data (*49*) on the Martian crust density (table S6). The depths (km) of the felsic crusts and protocrusts (Fig. 4) have been estimated based on the following equations (Eqs. 3 to 5)

$$H = \frac{P}{\rho\, g} \quad (3)$$

where *H* is the depth (km) of the partially melted system where the felsic crust is stable, *P* (Pa or kg m^{-1} s^{-2}) is the pressure of the thermodynamic stability of the felsic melts, ρ is the felsic crust density (2800 kg/m^3 for Earth and 2975 kg/m^3 for Mars) (*49*), and g is the gravitational constant (9.8 m/s^2 for Earth and 3.7 m/s^2 for Mars) (*59*)

$$F = \frac{m\ (\text{felsic melt})}{m\ (\text{crystal residue}) + m\ (\text{felsic melt})} \quad (4)$$

where *F* is the fraction of the melt in the hybrid system, *m* is mass (kg) of the felsic melt (equivalent of felsic crust), and the crystal residue is the crystals (olivine, chromite, and pyroxenes) in the produced hybrid systems

$$F = \frac{v\ (\text{felsic melt})}{V\ (\text{bulk system})} = \frac{h\ (\text{felsic crust})}{H\ (\text{bulk system})} \quad (5)$$

where *v* and *V* are the volumes of the produced felsic crust and the bulk partially melted system, respectively; and *h* and *H* are depths of the crust and the bulk partially melted system, respectively. The *H* (km) illustrated in Fig. 4 corresponds to the maximal pressures of the felsic melt and crust stability.

Supplementary Materials

The PDF file includes:

Figs. S1 to S7
Legends for tables S1 to S25
References

Other Supplementary Material for this manuscript includes the following:

Tables S1 to S25

REFERENCES AND NOTES

1. S. R. Taylor, S. McLennan, *Planetary Crusts: Their Composition, Origin and Evolution* (Cambridge Univ. Press, 2009), vol. 10.
2. I. H. Campbell, S. R. Taylor, No water, no granites—No oceans, no continents. *Geophys. Res. Lett.* **10**, 1061–1064 (1983).
3. H. Massol, A. Davaille, P. Sarda, Early formation of a water ocean as a function of initial CO_2 and H_2O contents in a solidifying rocky planet. *J. Geophys. Res. Planets* **128**, e2023JE007848 (2023).
4. V. Payré, M. R. Salvatore, C. S. Edwards, An evolved early crust exposed on Mars revealed through spectroscopy. *Geophys. Res. Lett.* **49**, e2022GL099639 (2022).
5. T. M. Harrison, *Hadean Earth* (Springer, 2020).
6. E. Hasenstab-Dübeler, J. Tusch, J. E. Hoffmann, M. Fischer-Gödde, K. Szilas, C. Münker, Temporal evolution of ^{142}Nd signatures in SW Greenland from high precision MC-ICP-MS measurements. *Chem. Geol.* **614**, 121141 (2022).
7. S. Volante, E. Blereau, M. Guitreau, M. Tedeschi, V. van Schijndel, K. Cutts, Current applications using key mineral phases in igneous and metamorphic geology: Perspectives for the future. *Geol. Soc. Lond. Spec. Publ.* **537**, 57–121 (2024).
8. E. A. Bell, P. Boehnke, T. M. Harrison, W. L. Mao, Potentially biogenic carbon preserved in a 4.1 billion-year-old zircon. *Proc. Natl. Acad. Sci. U.S.A.* **112**, 14518–14521 (2015).
9. B. Marty, The ancient Earth. *Geochem. Perspect.* **9**, 135–313 (2020).

10. D. Trail, T. M. McCollom, Relatively oxidized fluids fed Earth's earliest hydrothermal systems. *Science* **379**, 582–586 (2023).
11. O. Laurent, J. F. Moyen, J. F. Wotzlaw, J. Björnsen, O. Bachmann, Early Earth zircons formed in residual granitic melts produced by tonalite differentiation. *Geology* **50**, 437–441 (2022).
12. V. Sautter, M. J. Toplis, R. C. Wiens, A. Cousin, C. Fabre, O. Gasnault, S. Maurice, O. Forni, J. Lasue, A. Ollila, J. C. Bridges, N. Mangold, S. Le Mouélic, M. Fisk, P.-Y. Meslin, P. Beck, P. Pinet, L. Le Deit, W. Rapin, E. M. Stolper, H. Newsom, D. Dyar, N. Lanza, D. Vaniman, S. Clegg, J. J. Wray, In situ evidence for continental crust on early Mars. *Nat. Geosci.* **8**, 605–609 (2015).
13. V. Sautter, M. J. Toplis, P. Beck, N. Mangold, R. Wiens, P. Pinet, A. Cousin, S. Maurice, L. LeDeit, R. Hewins, O. Gasnault, C. Quantin, O. Forni, H. Newsom, P.-Y. Meslin, J. Wray, N. Bridges, V. Payré, W. Rapin, S. Le Mouélic, Magmatic complexity on early Mars as seen through a combination of orbital, in-situ and meteorite data. *Lithos* **254-255**, 36–52 (2016).
14. G. L. Hashimoto, M. Roos-Serote, S. Sugita, M. S. Gilmore, L. W. Kamp, R. W. Carlson, K. H. Baines, Felsic highland crust on Venus suggested by Galileo near-infrared mapping spectrometer data. *J. Geophys. Res. Planets* **113**, E00B24 (2008).
15. A. T. Basilevsky, E. V. Shalygin, D. V. Titov, W. J. Markiewicz, F. Scholten, T. Roatsch, M. A. Kreslavsky, L. V. Moroz, N. I. Ignatiev, B. Fiethe, B. Osterloh, H. Michalik, Geologic interpretation of the near-infrared images of the surface taken by the Venus Monitoring Camera, Venus Express. *Icarus* **217**, 434–450 (2012).
16. R. W. Nicklas, J. M. Day, K. G. Gardner-Vandy, A. Udry, Early silicic magmatism on a differentiated asteroid. *Nat. Geosci.* **15**, 696–699 (2022).
17. M. S. Phillips, C. E. Viviano, J. E. Moersch, A. D. Rogers, H. Y. McSween, F. P. Seelos, Extensive and ancient feldspathic crust detected across north Hellas rim, Mars: Possible implications for primary crust formation. *Geology* **50**, 1182–1186 (2022).
18. N. Drabon, B. L. Byerly, G. R. Byerly, D. R. Lowe, Heterogeneous Hadean crust with ambient mantle affinity recorded in detrital zircons of the Green Sandstone Bed, South Africa. *Proc. Natl. Acad. Sci. U.S.A.* **118**, e2004370118 (2021).
19. N. Drabon, B. L. Byerly, G. R. Byerly, J. L. Wooden, M. Wiedenbeck, J. W. Valley, K. Kitajima, A. M. Bauer, D. R. Lowe, Destabilization of long-lived Hadean protocrust and the onset of pervasive hydrous melting at 3.8 Ga. *AGU Adv.* **3**, e2021AV000520 (2022).
20. A. Y. Borisova, N. R. Zagrtdenov, M. J. Toplis, W. A. Bohrson, A. Nédélec, O. G. Safonov, G. S. Pokrovski, G. Ceuleneer, I. N. Bindeman, O. E. Melnik, K. P. Jochum, B. Stoll, U. Weis, A. Y. Bychkov, A. A. Gurenko, S. Shcheka, A. Terehin, V. M. Polukeev, D. A. Varlamov, K. Chariteiro, S. Gouy, P. de Parseval, Hydrated peridotite–basaltic melt interaction Part I: Planetary felsic crust formation at shallow depth. *Front. Earth Sci.* **9**, 640464 (2021).
21. A. Y. Borisova, A. Nédélec, N. R. Zagrtdenov, M. J. Toplis, W. A. Bohrson, O. G. Safonov, I. N. Bindeman, O. E. Melnik, G. S. Pokrovski, G. Ceuleneer, K. P. Jochum, B. Stoll, U. Weis, A. Y. Bychkov, A. A. Gurenko, Hadean zircon formed due to hydrated ultramafic protocrust melting. *Geology* **50**, 300–304 (2022).
22. K. H. Wedepohl, The composition of the continental crust. *Geochim. Cosmochim. Acta* **59**, 1217–1232 (1995).
23. Y. Amelin, D. C. Lee, A. N. Halliday, R. T. Pidgeon, Nature of the Earth's earliest crust from hafnium isotopes in single detrital zircons. *Nature* **399**, 252–255 (1999).
24. E. A. Belousova, Y. A. Kostitsyn, W. L. Griffin, G. C. Begg, S. Y. O'Reilly, N. J. Pearson, The growth of the continental crust: Constraints from zircon Hf-isotope data. *Lithos* **119**, 457–466 (2010).
25. A. I. S. Kemp, S. A. Wilde, C. J. Hawkesworth, C. D. Coath, A. Nemchin, R. T. Pidgeon, J. D. Vervoort, S. A. DuFrane, Hadean crustal evolution revisited: New constraints from Pb–Hf isotope systematics of the Jack Hills zircons. *Earth Planet. Sci. Lett.* **296**, 45–56 (2010).
26. T. Naeraa, A. Scherstén, M. T. Rosing, A. I. S. Kemp, J. E. Hoffmann, T. F. Kokfelt, M. J. Whitehouse, Hafnium isotope evidence for a transition in the dynamics of continental growth 3.2 Gyr ago. *Nature* **485**, 627–630 (2012).
27. E. A. Bell, T. M. Harrison, I. E. Kohl, E. D. Young, Eoarchean crustal evolution of the Jack Hills zircon source and loss of Hadean crust. *Geochim. Cosmochim. Acta* **146**, 27–42 (2014).
28. J. A. Mulder, O. Nebel, N. J. Gardiner, P. A. Cawood, A. N. Wainwright, T. J. Ivanic, Crustal rejuvenation stabilised Earth's first cratons. *Nat. Commun.* **12**, 3535 (2021).
29. S. S. Sun, W. F. McDonough, Chemical and isotopic systematics of oceanic basalts: Implications for mantle composition and processes. *Geol. Soc. Lond. Spec. Publ.* **42**, 313–345 (1989).
30. T. M. Harrison, E. A. Bell, P. Boehnke, Hadean zircon petrochronology. *Rev. Mineral. Geochem.* **83**, 329–363 (2017).
31. M. Guitreau, J. Blichert-Toft, Implications of discordant U-Pb ages on Hf isotope studies of detrital zircons. *Chem. Geol.* **385**, 17–25 (2014).
32. W. Chowdhury, D. Trail, M. Guitreau, E. Bell, J. Buettner, S. J. Mojzsis, Geochemical and textural investigations of the Eoarchean Ukaliq Supracrustals, Northern Québec (Canada). *Lithos* **372-373**, 105673 (2020).
33. O. Laurent, A. Zeh, A linear Hf isotope-age array despite different granitoid sources and complex Archean geodynamics: Example from the Pietersburg block (South Africa). *Earth Planet. Sci. Lett.* **430**, 326–338 (2015).
34. R. Latypov, S. Chistyakova, R. Grieve, H. Huhma, Evidence for igneous differentiation in Sudbury Igneous Complex and impact-driven evolution of terrestrial planet proto-crusts. *Nat. Commun.* **10**, 508 (2019).
35. O. Laurent, J. Björnsen, J. F. Wotzlaw, S. Bretscher, M. Pimenta Silva, J. F. Moyen, P. Ulmer, O. Bachmann, Earth's earliest granitoids are crystal-rich magma reservoirs tapped by silicic eruptions. *Nat. Geosci.* **13**, 163–169 (2020).
36. L. Manske, K. Wünnemann, K. Kurosawa, Quantification of impact-induced melt production in numerical modeling revisited. *J. Geophys. Res. Planets* **127**, e2022JE007426 (2022).
37. L. T. Elkins-Tanton, Magma oceans in the inner solar system. *Annu. Rev. Earth Planet. Sci.* **40**, 113–139 (2012).
38. T. Lyubetskaya, J. Korenaga, Chemical composition of Earth's primitive mantle and its variance: 1. Method and results. *J. Geophys. Res. Solid Earth* **112**, B03211 (2007).
39. B. L. Ehlmann, J. F. Mustard, S. L. Murchie, Geologic setting of serpentine deposits on Mars. *Geophys. Res. Lett.* **37**, L06201 (2010).
40. R. Wordsworth, A. H. Knoll, J. Hurowitz, M. Baum, B. L. Ehlmann, J. W. Head, K. Steakley, A coupled model of episodic warming, oxidation and geochemical transitions on early Mars. *Nat. Geosci.* **14**, 127–132 (2021).
41. V. Wright, M. Morzfeld, M. Manga, Liquid water in the Martian mid-crust. *Proc. Natl. Acad. Sci. U.S.A.* **121**, e2409983121 (2024).
42. T. Yoshizaki, W. F. McDonough, The composition of Mars. *Geochim. Cosmochim. Acta* **273**, 137–162 (2020).
43. M. A. Wieczorek, A. Broquet, S. M. McLennan, A. Rivoldini, M. Golombek, D. Antonangeli, C. Beghein, D. Giardini, T. Gudkova, S. Gyalay, C. L. Johnson, R. Joshi, D. Kim, S. D. King, B. Knapmeyer-Endrun, P. Lognonné, C. Michaut, A. Mittelholz, F. Nimmo, L. Ojha, M. P. Panning, A.-C. Plesa, M. A. Siegler, S. E. Smrekar, T. Spohn, W. Banerdt, InSight constraints on the global character of the Martian crust. *J. Geophys. Res. Planets* **127**, e2022JE007298 (2022).
44. N. H. Sleep, D. K. Bird, E. C. Pope, Serpentinite and the dawn of life. *Philos. Trans. R. Soc. London Ser. B Biol. Sci.* **366**, 2857–2869 (2011).
45. K. P. Jochum, B. Stoll, K. Herwig, M. Willbold, A. W. Hofmann, M. Amini, S. Aarburg, W. Abouchami, E. Hellebrand, B. Mocek, I. Raczek, A. Stracke, O. Alard, C. Bouman, S. Becker, M. Dücking, H. Brätz, R. Klemd, D. de Bruin, D. Canil, D. Cornell, C.-J. de Hoog, C. Dalpé, L. Danyushevsky, A. Eisenhauer, Y. Gao, J. E. Snow, N. Groschopf, D. Günther, C. Latkoczy, M. Guillong, E. H. Hauri, H. E. Höfer, Y. Lahaye, K. Horz, D. E. Jacob, S. A. Kasemann, A. J. R. Kent, T. Ludwig, T. Zack, P. R. D. Mason, A. Meixner, M. Rosner, K. Misawa, B. P. Nash, J. Pfänder, W. R. Premo, W. D. Sun, M. Tiepolo, R. Vannucci, T. Vennemann, D. Wayne, J. D. Woodhead, MPI-DING reference glasses for in situ microanalysis: New reference values for element concentrations and isotope ratios. *Geochem. Geophys. Geosyst.* **7**, Q02008 (2006).
46. K. P. Jochum, M. Willbold, I. Raczek, B. Stoll, K. Herwig, Chemical characterisation of the USGS reference glasses GSA-1G, GSC-1G, GSD-1G, GSE-1G, BCR-2G, BHVO-2G and BIR-1G Using EPMA, ID-TIMS, ID-ICP-MS and LA-ICP-MS. *Geostand. Geoanal. Res.* **29**, 285–302 (2005).
47. M. Guillong, D. L. Meier, M. M. Allan, C. A. Heinrich, B. W. Yardley, Appendix A6: SILLS: A MATLAB-based program for the reduction of laser ablation ICP-MS data of homogeneous materials and inclusions. *Mineral. Assoc. Can. Short Course Ser.* **40**, 328–333 (2008).
48. W. L. Griffin, "GLITTER: Data reduction software for laser ablation ICP-MS" in *Laser Ablation ICP-MS in the Earth Sciences: Current Practices and Outstanding Issues* (Mineralogical Association of Canada, 2008), pp. 308–311.
49. B. Knapmeyer-Endrun, M. P. Panning, F. Bissig, R. Joshi, A. Khan, D. Kim, V. Lekić, B. Tauzin, S. Tharimena, M. Plasman, N. Compaire, R. F. Garcia, L. Margerin, M. Schimmel, É. Stutzmann, N. Schmerr, E. Bozdağ, A.-C. Plesa, M. A. Wieczorek, A. Broquet, D. Antonangeli, S. M. M. Lennan, H. Samuel, C. Michaut, L. Pan, S. E. Smrekar, C. L. Johnson, N. Brinkman, A. Mittelholz, A. Rivoldini, P. M. Davis, P. Lognonné, B. Pinot, J.-R. Scholz, S. Stähler, M. Knapmeyer, M. van Driel, D. Giardini, W. B. Banerdt, Thickness and structure of the Martian crust from InSight seismic data. *Science* **373**, 438–443 (2021).
50. M. Collinet, A. C. Plesa, T. Ruedas, S. Schwinger, D. Breuer, The temperature and composition of the mantle sources of Martian basalts. *Geophys. Res. Lett.* **50**, e2023GL103537 (2023).
51. B. M. Tutolo, N. J. Tosca, Observational constraints on the process and products of Martian serpentinization. *Sci. Adv.* **9**, eadd8472 (2023).
52. M. S. Ghiorso, R. O. Sack, Chemical mass transfer in magmatic processes IV. A revised and internally consistent thermodynamic model for the interpolation and extrapolation of liquid-solid equilibria in magmatic systems at elevated temperatures and pressures. *Contrib. Mineral. Petrol.* **119**, 197–212 (1995).

53. G. A. Gualda, M. S. Ghiorso, R. V. Lemons, T. L. Carley, Rhyolite-MELTS: A modified calibration of MELTS optimized for silica-rich, fluid-bearing magmatic systems. *J. Petrol.* **53**, 875–890 (2012).
54. T. J. B. Holland, R. T. J. B. Powell, An internally consistent thermodynamic data set for phases of petrological interest. *J. Metam. Geol.* **16**, 309–343 (1998).
55. T. J. B. Holland, E. Green, R. Powell, Melting of peridotites through to granites: A simple thermodynamic model in the system KNCFMASHTOCr. *J. Petrol.* **59**, 881–900 (2018).
56. R. W. White, R. Powell, T. E. Johnson, The effect of Mn on mineral stability in metapelites revisited: New *a–x* relations for manganese-bearing minerals. *J. Metam. Geol.* **32**, 809–828 (2014).
57. A. Bouvier, J. D. Vervoort, P. J. Patchett, The Lu-Hf and Sm-Nd isotopic composition of CHUR: Constraints from unequilibrated chondrites and implications for the bulk composition of terrestrial planets. *Earth Planet. Sci. Lett.* **273**, 48–57 (2008).
58. E. Scherer, C. Münker, K. Mezger, Calibration of the lutetium-hafnium clock. *Science* **293**, 683–687 (2001).
59. C. V. Voorhies, T. J. Sabaka, M. Purucker, On magnetic spectra of Earth and Mars. *J. Geophys. Res. Planets* **107**, 1-1-1-10 (2002).
60. T. Iizuka, T. Yamaguchi, Y. Hibiya, Y. Amelin, Meteorite zircon constraints on the bulk Lu−Hf isotope composition and early differentiation of the Earth. *Proc. Natl. Acad. Sci. U.S.A.* **112**, 5331–5336 (2015).
61. M. Guitreau, J. Blichert-Toft, H. Martin, S. J. Mojzsis, F. Albarède, Hafnium isotope evidence from Archean granitic rocks for deep-mantle origin of continental crust. *Earth Planet. Sci. Lett.* **337**, 211–223 (2012).
62. R. B. Emo, M. A. Smit, M. Schmitt, E. Kooijman, E. E. Scherer, P. Sprung, W. Bleeker, K. Mezger, Science direct evidence for evolved Hadean crust from Sr isotopes in apatite within Eoarchean zircon from the Acasta Gneiss complex. *Geochim. Cosmochim. Acta* **235**, 450–462 (2018).
63. M. Guitreau, M. Boyet, J.-L. Paquette, A. Gannoun, Z. Konc, M. Benbakkar, K. Suchorski, J.-M. Hénot, Hadean protocrust reworking at the origin of the Napier Complex (Antarctica). *Geochem. Perspect. Lett.* **12**, 7–11 (2019).
64. A. Gerdes, A. Zeh, Zircon formation versus zircon alteration—New insights from combined U-Pb and Lu-Hf in-situ LA-ICP-MS analyses, and consequences for the interpretation of Archean zircon from the central zone of the Limpopo belt. *Chem. Geol.* **261**, 230–243 (2009).
65. A. Buzenchi, H. Moreira, O. Bruguier, D. Bosch, B. Dhuime, High spatial resolution (10–50 mm) analysis of Sr isotopes in rock-forming apatite by LA-MC-ICPMS. *J. Anal. At. Spectrom* **38**, 2113–2126 (2023).
66. R. Doucelance, E. Bruand, S. Matte, C. Bosq, D. Auclair, A. Gannoun, In-situ determination of Nd isotope ratios in apatite by LA-MC-ICPMS: Challenges and limitations. *Chem. Geol.* **550**, 119740 (2020).
67. C. M. Fisher, A. M. Bauer, J. D. Vervoort, Disturbances in the Sm–Nd isotope system of the Acasta Gneiss complex—Implications for the Nd isotope record of the early Earth. *Earth Planet. Sci. Lett.* **530**, 115900 (2020).

Acknowledgments: We did not use any editing services or AI-assisted technologies in the preparation of this manuscript. We thank the editors and the reviewers for important suggestions on the initial version of the paper. **Funding:** M.G. acknowledges funding from ClerVolc (ANR-10-LABX-0006). This manuscript is contribution no. 683 of the ClerVolc program of the International Research Center for Disaster Sciences and Sustainable Development of the University Clermont Auvergne. A.Y.B. thank funding PLAGIOGRAN grant from INSU-CNRS and FELSIC_PLANETA from OMP, France. This article is funded by the European Union (ERC, PLANETAFELSIC, project 101141259) to A.Y.B. Views and opinions expressed are, however, those of the author(s) only and do not necessarily reflect those of the European Union or EUROPEAN RESEARCH COUNCIL EXECUTIVE AGENCY (ERCEA). Neither the European Union nor the granting authority can be held responsible for them. **Author contributions:** Conceptualization: A.Y.B., M.G., A.N., W.A.B., and O.G.S. Data curation: A.Y.B., M.G., and O.G.S. Methodology: A.Y.B., M.G., J.B., O.G.S., and W.A.B. Resources: A.Y.B. and M.G. Investigation: A.Y.B., J.B., M.G., O.G.S., S.A.K., P.A., and P.P. Visualization: J.B., A.Y.B., M.G., and S.A.K. Funding acquisition: A.Y.B. Formal analysis: J.B., A.Y.B., M.G., and P.P. Project administration: A.Y.B. Software: P.A. and W.A.B., Supervision: A.Y.B. and P.A., Validation: A.Y.B., M.G., O.G.S., S.A.K., and P.P. Writing—original draft: A.Y.B., M.G., W.A.B., J.B., and O.G.S. Writing—review and editing: A.Y.B., M.G., W.A.B., A.N., J.B., and O.G.S. **Competing interests:** The authors declare that they have no competing interests. **Data and materials availability:** All data needed to evaluate the conclusions in the paper are present in the paper and/or the Supplementary Materials.

Submitted 23 August 2024
Accepted 24 February 2025
Published 26 March 2025
10.1126/sciadv.ads6746